Group: Magnetohydrodynamics

Magnetohydrodynamics for liquid-metal blankets

L. Bühler, H.-J. Brinkmann, V. Klüber, C. Köhly, C. Mistrangelo

Numerical simulations of 3D magnetohydrodynamic flows for dual-coolant lead lithium blankets

The dual coolant lead lithium (DCLL) blanket is one of the liquid metal blanket concepts foreseen in a DEMOnstration nuclear fusion reactor. The liquid metal serves here as breeder, neutron multiplier, neutron shield and as coolant to remove the volumetrically generated heat. The movement of the electrically conducting fluid in the strong magnetic field induces electric currents responsible for strong Lorentz forces, high magnetohydrodynamic (MHD) pressure drop, with implications on heat and mass transfer. The current density in the fluid can be reduced by decoupling electrically the liquid metal from the well-conducting blanket structure by thin-walled flow channel inserts (FCI) as proposed for the DCLL concept [1]. Sandwich-type FCIs consist of an electrically insulating ceramic layer protected from all sides by thin sheets of steel to avoid direct PbLi-ceramic contact. The steel layers are thin to provide sufficient Ohmic resistance for limiting currents. In order to support design activities for DCLL blankets, 3D numerical MHD simulations have been performed for pressure driven MHD flows in a DCLL blanket duct (Fig. 1). The liquid metal enters the blanket structure radially at the bottom, flows in a poloidal channel along the plasma-facing first wall, makes a U-turn at the top and flows down in a second poloidal duct before it leaves the module through the back plate. Fig. 1 shows the design of a DCLL blanket module and the simplified model used for the numerical simulations.

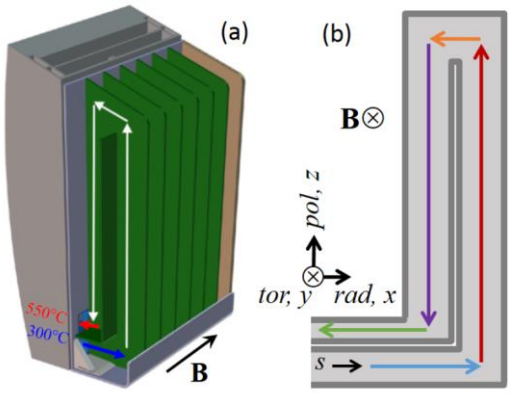

Fig. 1 Design of a DCLL blanket module [2] (a) and principle sketch of flow path (b).

The physical parameters characterizing the MHD flow are the Hartmann number and the Reynolds number,

$$Ha = BL\sqrt{\frac{\sigma}{\rho\nu}}, \quad Re = \frac{u_0 L}{\nu},$$

where L and u_0 denote typical length scale and velocity. Ha^2 und Re stand for the ratio of electromagnetic to viscous forces and inertia to viscous forces, respectively. In the present work L=0.0808m stands for half the duct size measured in toroidal direction and u_0 is the average velocity at the inlet. The conductance of the FCI has been taken into account by numerically resolving the thin conducting sheets with thickness t_w=0.5mm [2]. The computational mesh with $5.7 \cdot 10^6$ cells consists of structured hexahedral cells with non-uniform spacing for higher resolution of boundary layers and conducting sheets of the FCIs. The lengths of entrance and exit ducts have been extended compared with the original design in order to impose fully established entrance conditions

and reasonable convective parallel outflow. The numerical method uses an extension of the hydrodynamic open source code OpenFOAM for MHD applications [3].

Figure 2 shows contours of electric potential and velocity streamlines in the model geometry at the mid-plane of the duct for moderate *Ha*=500 and fusion-relevant high *Ha*=8000. 3D effects are present near bends and U-turn, but the flow approaches quite rapidly fully established conditions in the poloidal channels. Streamlines follow approximately lines of constant electric potential. Flow separation and recirculation, visible for *Ha*=500 behind the bends, are suppressed for higher magnetic fields. Despite the high Reynolds number *Re*=10932 the flow remains stable and laminar for the parameters considered.

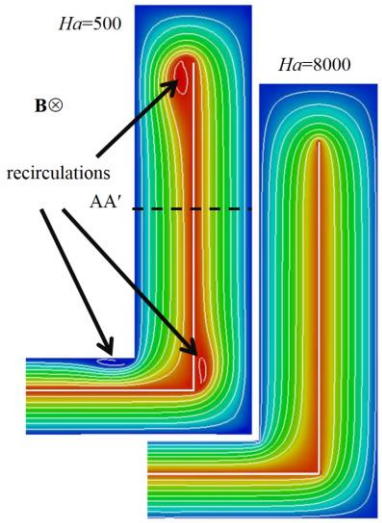

Fig. 2 Contours of potential and streamlines in a DCLL blanket for u0=2cm/s, for Ha=500 and Ha=8000.

The pressure distribution along a centerline of the blanket module is shown in Figure 3 for *Ha*=8000 and two velocities u_0=1cm/s and u_0=2cm/s. Bends and U-turns do not substantially contribute to the total pressure drop, because the flow turns in radial-poloidal planes perpendicular to **B** [4]. Immediately after passing 3D elements, the pressure gradient practically coincides with that of an asymptotic analysis for fully developed flows.

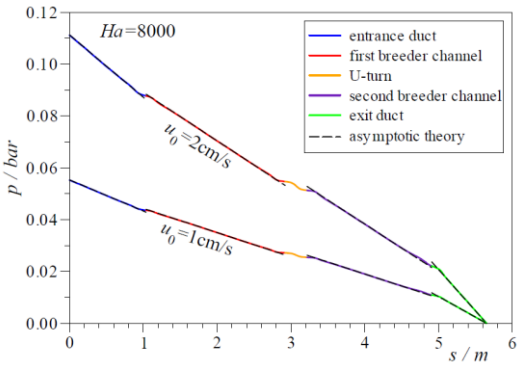

Fig. 3 Pressure as a function of a coordinate *s* along the flow path in the center of the channels.

Simulations for various Hartmann numbers $500 \le Ha \le 8000$ and flow rates show that the total pressure drop scales as $\Delta p \sim u_0 B^2$, the typical scaling for inertialess MHD flows in strong magnetic fields. Present results, published in [5], should be considered as a first step for predicting liquid metal flow in DCLL blankets. In order to complement the present work, future simulations will take into account in addition inclined fields, heat transfer and strong buoyancy effects for which the laminar flow might become unstable or even turbulent.

Experimental study of liquid metal MHD flows near gaps between FCIs

For reduction of pressure drop in DCLL blankets, electrically insulating flow channel inserts (FCIs) are foreseen for electrically decoupling the liquid metal flow from the well-conducting channel walls. For fabrication reasons, gaps between inserts are unavoidable. Gaps interrupt the electrical insulation, thus providing unwanted local short circuit for electric currents. For experimental investigations of 3D effects at junctions of FCIs, a test section has been man-

ufactured and experiments are currently performed in the MEKKA facility [6] using NaK as model fluid. The experimental study shows the benefits of FCIs for pressure drop reduction in fully developed flows as also predicted by theoretical analyses [7] and quantifies the deterioration of pressure drop reduction by the presence of uninsulated gaps between FCIs.

The test section used for experimental investigations has a circular cross-section. Details of the geometry and dimensions, including the radius R_{FCI} of the inner steel layer of the FCI, are shown in Figure 4. The thick-walled pipe has an inner radius $R=L$ that is used as length scale for the problem. The thickness t_{FCI}=0.5mm of the protection sheets has been suggested e.g. in [2]. More details about the instrumentation and first results can be found in [8].

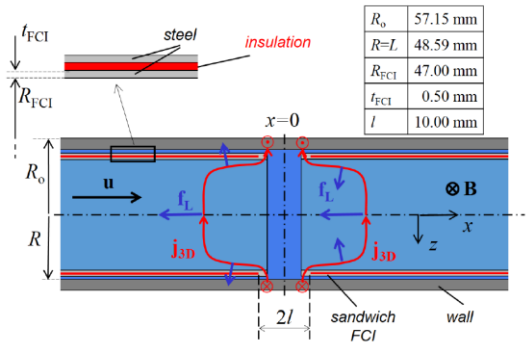

Fig. 4 Geometry at the junction between two FCIs.

The intensity of the flow and strength of the magnetic field are quantified by the non-dimensional Reynolds and Hartmann numbers Re and Ha. The influence of wall conductivity σ_w on MHD pipe flow is described using the wall conductance parameter c according to [9], which evaluates for the present problem and material properties at 50°C to

$$c = \frac{\sigma_w}{\sigma}\frac{R_0^2 - R^2}{R_0^2 + R^2} = 0.0727$$

for the thick-walled pipe and to c_{FCI}=0.00476 for the thin inner conducting sheet of the FCI. For strong magnetic fields, the nondimensional pressure gradients in fully established flow become $\partial p/\partial x$=0.0678 for the pipe without FCI and to $\partial p/\partial x$=0.00508 for an infinitely long FCI, respectively [8].

For investigations of 3D effects near the non-insulated region at x=0, the gap between FCIs has been positioned in the center of the magnet. Pressure differences with respect to the position x=0 have been measured along the axis and normalized by $\sigma u_0 B^2 L$. In the following, x stands for the axial position, scaled by L. The insulations in both FCIs extend from x=±0.2 up to x=±12.25 as illustrated in the subplot in Fig. 5Figure 5.

Results displayed in Figure 5 for Ha=3000 show the great benefit from using FCIs by comparing the theoretical curves for pipe flow and assumed perfect FCI. The theory for fully developed MHD flows predicts a pressure drop reduction factor of 0.0678/0.00508=13.3. At some distance from the gap, here for $|x|>1$, the measured pressure gradients in the FCIs are close to these predictions as indicated in the figure. Experiments confirm that a pressure drop reduction close to theoretical values is achievable with the used sandwich-type inserts. At larger distance from the center, the pressure gradient increases. This is caused by additional 3D effects, since for $|x|>8.8$ the magnetic field is not uniform anymore and the insulation ends at $|x|$=12.24. 3D effects at entrance and exit of FCIs will be investigated in future experiments. At x=0 some additional pressure drop Δp_{3D}=0.12 is present due to leakage currents across the gap into the well-conducting pipe wall. There seems to be no difference in non-dimensional pressure drop near the gap for the Reynolds numbers considered, i.e. those flows are apparently inertialess.

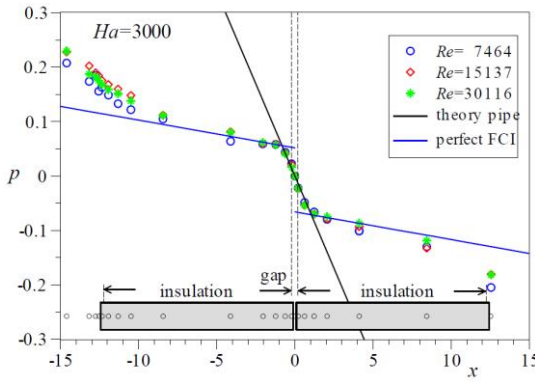

Fig. 5 MHD flow at the junction between two FCIs. Pressure along the axis for *Ha*= 3000 and different *Re*. Positions of FCIs and pressure taps are illustrated in the sketch.

According to these results, sandwich-type FCIs may reduce pressure drop of fully developed MHD flow by more than one order of magnitude compared to that in a thick-walled pipe. The additional non-dimensional pressure drop at a gap between two FCIs Δp_{3D}=0.12 seems not very high. Nevertheless, one should keep in mind that this pressure drop caused by one single non-insulated gap corresponds to that of a fully developed flow in an FCI over a length Δl_{3D}=23.6.

Fabrication of thin-walled flow channel inserts

Manufacturing of straight rectangular sandwich-type FCIs for DCLL blankets have been achieved by standard technologies such as coating, bending and welding [10]. However, it turned out that these techniques cannot be applied to circular FCIs as required in the experiments described above. The fabrication of sandwich-type FCIs for geometries deviating from rectangular cross section requires a different method, which has been developed. The process starts with a thin-walled pipe as inner sheet. The latter is coated on the outer surface with an insulating ceramic layer leaving blank small areas at both ends and a narrow stripe along the pipe (see Figure 6). A second metal sheet is wrapped around the coated pipe and laser-welded along all edges. The small longitudinal non-coated stipe foreseen in the experiment for measurement purposes (pressure taps) would not be required for FCIs in blanket ducts. After successful fabrication, the FCIs have been exposed to high temperatures above 300°C. Afterwards all welds have been checked by a dye penetrant test, which did not show any crack or defect. One prototype FCI has been cut into pieces for microscopic inspection of weld samples. The welds in all samples show no cracks or pores and a difference with respect to the original material could not be seen. More details about the fabrication of this circular FCI can be found in [11]. The method proposed here (coating, wrapping, welding), proven to be efficient for fabrication of circular FCIs, should apply as well for other types of cross section shapes that do not have sharp corners.

Fig. 6 Pipe coated with SilCor®SiC (left), wrapped and laser-welded (right).

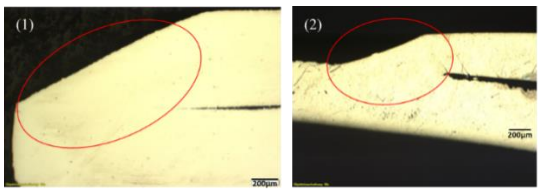

Fig. 7 Samples of polished specimens: (1) edge of the orbital weld, (2) longitudinal weld.

The fabrication of insulating 3D components like complex shaped FCIs for DCLL blankets is more challenging. Selective laser melting (SLM) is an additive manufacturing technique,

in which a high-power-density laser melts metallic powders gradually in layers to create solid 3D structures. This technique has been tested for fabrication of complex thin and double-walled insulating 3D FCIs. Preliminary studies for SLM-produced components have been made to check material properties and to fabricate hybrid elements for blankets such as stiffening plates with cooling channels [12], [13].

The FCIs produced by SLM have been designed as a downscaled model of a liquid metal channel in the DCLL blanket (Figure 8Fig. 8). The 3D shape of the mockup follows the liquid metal flow path inside the blanket. Objective is to show the general feasibility of fabricating complex 3D double-walled FCI structures with very thin walls by SLM. Walls should be as thin as currently achievable with SLM and produced from reduced activation martensitic Cr-Mo steel Eurofer97. The fact that Eurofer97 is not a standard material for SLM and walls should be as thin as possible, poses a major challenge for the manufacturer. The first mockup therefore is considered as a test to gain experience about practical limitations of present-day SLM technique. The FCI model has been designed with a height of 110mm. It consists of a double-walled structure with 0.8mm wall thickness each and an insulating gap of 0.8mm. The inner and outer walls are initially separated from each other by spacers at both openings to ensure exact positioning of both walls. After completion of the model by SLM, the gap between the layers has been filled with ceramic powder (ø0.3mm), the spacers have been removed and the gaps were closed by non-conducting caps (Fig. 9).

Inspection of this first FCI mockup shows that some of the walls have certain deformations. Electrical resistance measurements confirm undesired contacts. Examinations by x-ray computed tomography (CT) show the positions, where inner and outer walls might be in contact and deteriorate the electrical isolation.

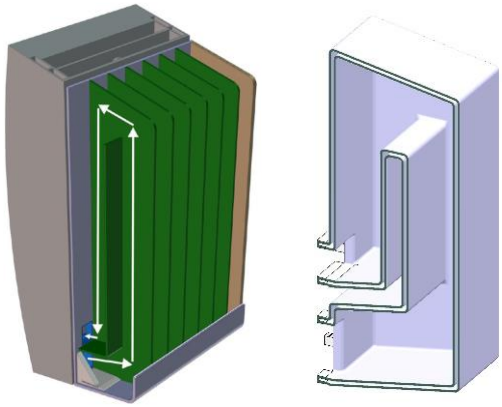

Fig. 8: Present design of DCLL blanket (left) [2] and CAD model of the downscaled double-walled SLM-fabricated FCI mockup (right).

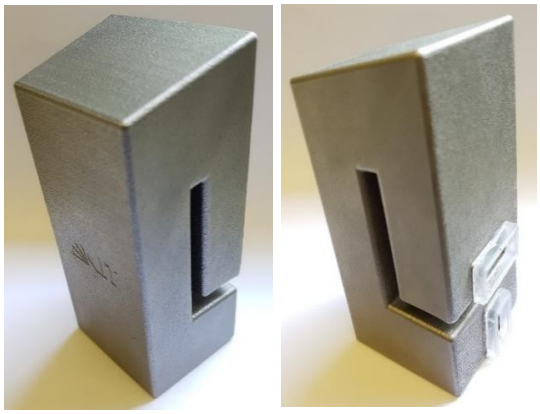

Fig. 9: FCI filled-up with ceramic powder and closed by caps.

After optimization of the SLM process, a second mockup has been fabricated with slightly increased thickness of 1mm for each wall and an insulating gap of 1.4mm. It has been observed and confirmed by CT scans, that walls are now much less deformed (see Figure 10). Electric resistance measurements confirm perfect electrical insulation and therewith ensured full functionality of the mockup for electrically decoupling of the liquid metal flow from the well conducting blanket structure. For more details see [14].

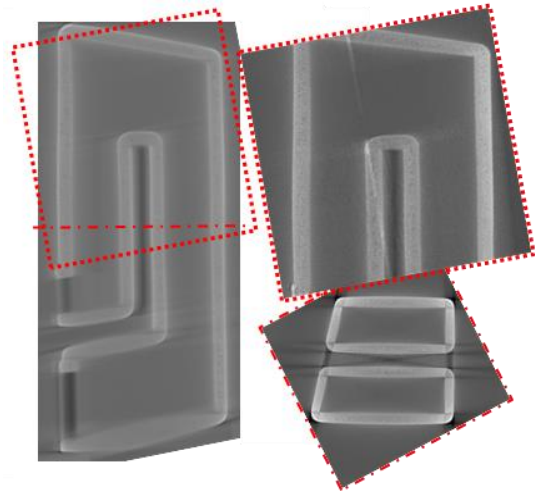

Fig. 10: CT scan of the improved FCI mockup (1mm wall thickness, 1.4 mm nominal gap): Longitudinal cut (left), detail (right, top), cross section (right, bottom). (*by Andreas Meier, KIT-IAM*)

The present work should be considered as proof of suitability for production of 3D sandwich-type insulating elements for liquid metal blankets, based on available technology for SLM. For fabrication of full-scale components, SLM machines would require new approaches [13] and upscaling in dimensions.

Design of a test section for analysis of magneto-convection in water-cooled lead lithium blankets

Another liquid metal blanket concept considered for a DEMO reactor is the water-cooled lead lithium (WCLL) breeding blanket [15]. The liquid metal alloy lead lithium PbLi is used as breeder, neutron multiplier and as heat carrier. Pressurized water flows through a large number of cooling pipes immersed in the liquid metal and cools the walls and breeding zone (see Figure 11). In order to get first insight in the distribution of the PbLi flow resulting from the combined interaction of electromagnetic forces, buoyancy and pressure, preliminary numerical and experimental studies of buoyant MHD flows are foreseen. A simplified model geometry will be used for these studies to improve the understanding of magneto-convective flows and to demonstrate the feasibility of the proposed WCLL DEMO design. First results for flows in vertical channels with internal obstacles have been reported in [16].

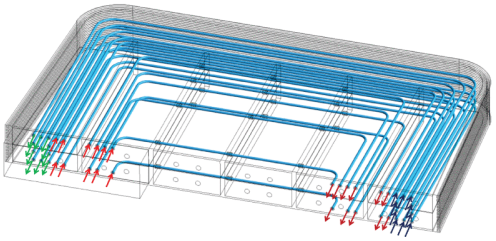

Fig. 11 WCLL blanket (ENEA [14]), equatorial section in a blanket module with cooling pipes.

Figure 12 shows the CAD design of the experimental test section. It consists of a liquid-metal-filled box, in which a heated pipe simulates neutron heating while a cooled pipe removes the heat from the liquid metal. The magneto-convective flow is driven by buoyancy, when heat is exchanged between liquid metal and the cooling and heating pipes. The dimensions of the box have been chosen such that the experiment fits into the gap of the dipole magnet available in the MEKKA laboratory.

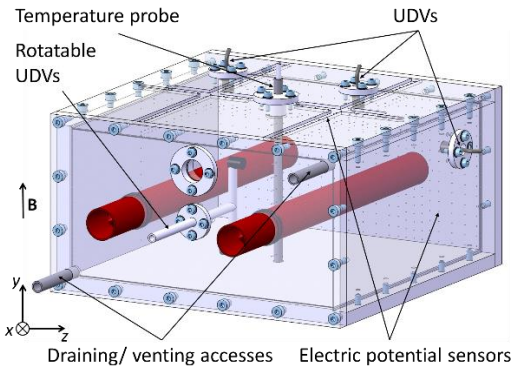

Fig. 12 Design of the experimental test section.

The pipes are supplied with copper cores for achieving as good as possible isothermal conditions. Thermocouples at different axial and circumferential positions monitor the temperature during the experiments near the inlet, outlet and at the center of the pipes (see Figure 13).

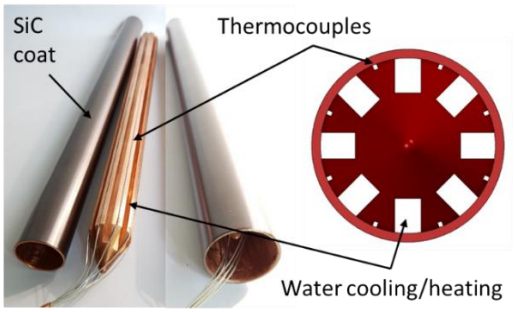

Fig. 13 Copper pipe and core with inserted thermocouples (left), front view of design (right).

In order to support the design of the present model experiment with some theoretical data, numerical simulations have been performed, in which the driving temperature difference between heated and cooled pipe has been set to ΔT=T2-T1=40K. The strength of the magnetic field is measured in terms of the Hartmann number *Ha*. All walls are electrically insulating and adiabatic. Some results of numerical simulations are shown in Figure 14. The figures in the left column show contours of fluid temperature. Flow streamlines indicate that there are convective cells present in the center between the two pipes and the maximum velocity occurs near the walls of the tubes. According to these results, suitable positions for measuring temperature are along magnetic field lines. Interesting velocity data is expected in layers tangent to the pipes, and electric potential differences might be seen only on the end walls of the box, where electric currents have to close in thin viscous layers.

The temperature distribution in the center of the test section is measured by a temperature probe with 11 thermocouples equidistantly distributed over the height (Figure 15). The temperature on the walls of the box is monitored in more than 50 positions in order to get an overview of the temperature distribution and to estimate the amount of transferred heat.

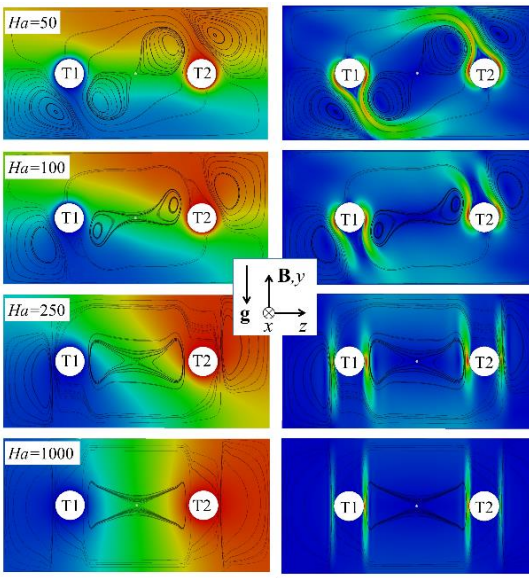

Fig. 14 Magneto-convective flow for ΔT=T2-T1=40K. Contours of temperature (left) and magnitude of velocity (right).

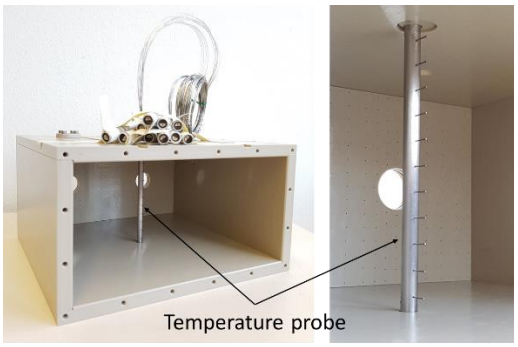

Fig. 15 Temperature probe in the test section.

The electric potential will be measured on the fluid-solid interface by a large number of copper electrodes that penetrate specific walls of the test section. Most interesting walls, the end walls, are instrumented with a dense population of electrodes.

Numerical simulations show that the highest velocities occur in thin layers tangent to the heating/cooling pipes. It is planned to record velocity data from those layers by using Ultrasound Doppler Velocimetry (UDV) [17]. A principle sketch showing the positions of the sensors and the propagation zones of the ultrasonic pulses is displayed in Figure 16. Two sensors will give information about the flow in the tangent layers and one in the cores. For measuring velocity along other directions, a movable probe with two UDV sensors is foreseen. The probe is mounted on a rotatable rod and can be turned in *yz* plane.

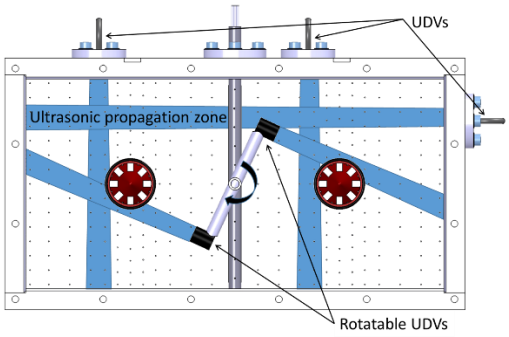

Fig. 16 Sketch showing positions of UDV sensors on the walls and rotatable probe. Propagation zones of ultrasonic pulses in blue.

Before the test section will be filled with liquid metal, first experiments are performed using water as a test fluid. These preliminary tests are foreseen to show full functionality of the instrumentation, and they will give first results for the hydrodynamic limit, when no magnetic field is present. Water allows optical access and application of Particle Image Velocimetry (PIV) for flow visualization. For this purpose, end walls and one sidewall are replaced by transparent material (see Figure 17).

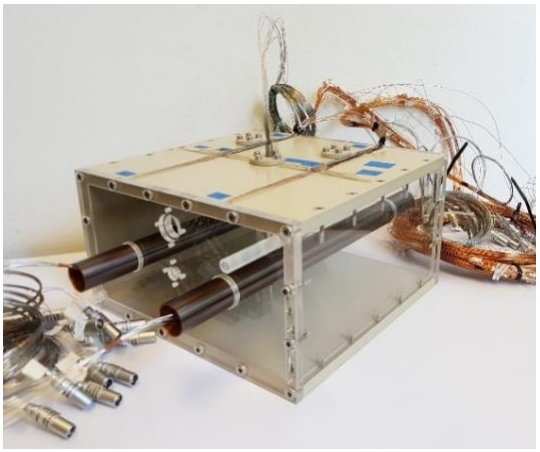

Fig. 17 WCLL mockup for preliminary experiments with water: front, side and back walls made of Plexiglas.

The test section is now instrumented and ready for measuring simultaneously temperature, potential and velocity distribution. It is foreseen to perform experiments in 2019 for various values of the applied magnetic field and driving temperature differences, i.e. for various Hartmann and Grashof numbers, respectively.

Further work

In addition to the topics described above, the MHD group at IKET KIT contributed in reporting period 2017-2018 with scientific papers to the development of helium cooled lead lithium (HCLL) blankets [18], [19], [20] [21], [22], to sensor development [23], and to fundamental studies of MHD flows [24], [25], [26], [27], [28], [29], [30].

References

[1] Rapisarda, D., Fernandez, I.; Palermo, I.; Urgorri, F.; Maqueda, L.; Alonso, D.; Melichar, T.; Frýbrt, O.; Vála, L.; Gonzalez, M.; Norajitra, P.; Neuberger H. and Ibarra, A.; "Status of the engineering activities carried out on

the European DCLL," Fusion Engineering and Design, 2017.

[2] Fernández-Berceruelo, I.; Gonzalez, M.; Palermo, I.; Urgorri F. and Rapisarda, D.; "Large-scale behavior of sandwich-like FCI components within the EU-DCLL operational conditions," Fusion Engineering and Design, p. in print, 2018.

[3] Mistrangelo, C. and Bühler, L.; "Development of a numerical tool to simulate magnetohydrodynamic interactions of liquid metals with strong applied magnetic fields," Fusion Science and Technology, vol. 60, no. 2, pp. 798-803, 2011.

[4] Molokov, S.; "Liquid metal flows in manifolds and expansions of insulating rectangular ducts in the plane perpendicular to a strong magnetic field," 1994.

[5] Klüber, V.; Mistrangelo, C. and Bühler, L.; "Numerical simulations of 3D magneto-hydrodynamic flows for dual-coolant lead lithium blankets," in Proceedings of the 30th Symposium on Fusion Technology SOFT, Giardini Naxos, Italy, September 16-21, 2018, 2018.

[6] Barleon, L. ; Mack, K.-J. and Stieglitz, R.; "The MEKKA-facility a flexible tool to investigate MHD-flow phenomena," 1996.

[7] Bühler, L. and Mistrangelo, C.; "Pressure drop and velocity changes in MHD pipe flows due to a local interruption of the insulation," Fusion Engineering and Design, vol. 127, pp. 185-191, 2018.

[8] Bühler, L.; Brinkmann, H.-J. and Koehly, C.; "Experimental study of liquid metal magnetohydrodynamic flows near gaps bet-ween flow channel inserts," in Proceedings of the 30th Symposium on Fusion Technology SOFT, Giardini Naxos, Italy, September 16-21, 2018, 2018.

[9] Miyazaki, K.; Konishi, K. and Inoue, S.; "MHD pressure prop of liquid metal flow in circular duct under variable transverse magnetic field," Journal of Nuclear Science and Technology, vol. 28, no. 2, pp. 159-161, 1991.

[10] Norajitra, P.; Basuki, W.W.; Gonzalez, M.; Rapisarda, D.; Rohde, M. and Spatafora, L.; "Development of sandwich flow channel inserts for an EU DEMO dual coolant blanket concept," Fusion Science & Technology, vol. 68, no. 3, pp. 501-506, 2015.

[11] Koehly, C. and Bühler, L.; "Fabrication issues of sandwich-like flow channel inserts for circular pipes," Fusion Science and Technology, vol. 72, pp. 660-666, 2017.

[12] Neuberger, H.; Rey, J.; Hees, M.; Materna-Morris, E.; Bolich, D.; Aktaa, J.; Meier, A.; Fischer, S.; Schorle, C.; Fuhrmann, U.; Heger, R.; Dlouhy, I.; Stratil, L. and Kloetzer, B.; "Selective laser sintering as manufacturing process for the realization of complex nuclear fusion and high heat flux components," Fusion Science and Technology, vol. 72, no. 4, pp. 667-672, 2017.

[13] Neuberger, H.; Rey, J.; Hernandez, F.; Ruck, S.; Arbeiter, F.; Rieth, M.; Koehly, C.; Stratil, L.; Niewoehner, R. and Felde, A.; "Evaluation of conservative and innovative manufacturing routes for gas cooled Test Blanket Module and Breeder Blanket First Walls," in Proceedings of the 30th Symposium on Fusion Technology SOFT, Giardini Naxos, Italy, September 16-21, 2018, 2018.

[14] Koehly, C.; Neuberger, H. and Bühler, L.; "Fabrication of thin-walled fusion blanket components like flow channel inserts by selective laser manufacturing," in Proceedings of the 30th Symposium on Fusion Technology SOFT, Giardini Naxos, Italy, September 16-21, 2018, 2018.

[15] Romanelli, F.; Barabaschi, P.; Borba, D.; Federici, G.; Horton, L.; Neu, R.; Stork, D. and Zohm, H.; "Fusion electricity: A roadmap to the realisation of fusion energy," EFDA, 2012.

[16] Bühler, L. and Mistrangelo, C.; "MHD flow and heat transfer in model geometries for WCLL blankets," Fusion Engineering and Design, vol. 122, pp. 919-923, 2017.

[17] Brito, D.; Nataf, H.-C.; Cardin, P.; Aubert, J. and Masson, J.-P.; "Ultrasonic Doppler Velocimetry in Liquid Gallium," Experiments in Fluids, vol. 31, pp. 653-663, 2001.

[18] Bühler, L.; Mistrangelo, C.; Brinkmann, H.-J. and Koehly, C.; "Pressure distribution in MHD flows in an experimental test-section for a HCLL blanket," Fusion Engineering and Design, vol. 127, pp. 168-172, 2018.

[19] Mistrangelo, C. and Büher, L.; "Determination of multichannel MHD velocity profiles from wall-potential measurements and numerical simulations," Fusion Engineering and Design, vol. 130, pp. 137-141, 2018.

[20] Mistrangelo, C.; Bühler, L. and Brinkmann, H.-J.; "Experimental investigation of MHD pressure losses in a mock-up of a liquid metal blanket," Nuclear Fusion, vol. 58, p. 036012, 2018.

[21] Mistrangelo, C.; Bühler, L.; Koehly, C. and Brinkmann, H.-J.; "Influence of modifications of HCLL blanket design on MHD pressure losses," Fusion Engineering and Design, vol. 124, pp. 948-952, 2017.

[22] Mistrangelo, C. and Bühler, L.; "Magnetohydrodynamic flows in liquid metal blankets for fusion reactors," Proceedings in Applied Mathematics and Mechanics, vol. 17, pp. 115-118, 2017.

[23] Bühler, L.; Aiello, G.; Bendotti, S.; Koehly, C.; Mistrangelo, C. and Galabert, J.; "Development of combined temperature – electric potential sensors," Fusion Engineering and Design, vol. 136, pp. 7-11, 2018.

[24] Arlt, T.; "Analyse des Stabilitätsver-haltensmagnetohydrodynamischer Kanalströmungen," PhD Thesis, Karlsruhe Institute of Technology, 2018.

[25] Krasnov, D.; Bandaru, V.; Bühler, L. and Boeck, T.; "Instabilities and turbulence in magnetohydrodynamic duct flows," in Proceedings of the NIC Symposium 2018. 22-23.02.2018, Jülich, Germany, vol. 49, K. Binder, M. Müller and A. Trautmann, Eds., Jülich, Germany, John-von-Neumann Institute for Computing, 2018, pp. 389-396.

[26] Arlt, T.; Priede, J. and Bühler, L.; "Influence of thin finitely conducting walls on the linear stability of magnetohydrodynamic flows," Magnetohydrodynamics, vol. 53, no. 1, pp. 35-44, 2017.

[27] Arlt, T.; Priede, J. and Bühler, L.; "The effect of finite-conductivity Hartmann walls on the linear stability of Hunt's flow," Journal of Fluid Mechanics, vol. 822, pp. 880-891, 2017.

[28] Chowdhury, V.; "Experimentelle Untersuchungen von magnetohydrodynamisch induzierten Instabilitäten," PhD Thesis, Karlsruhe Institute of Technology, 2017.

[29] Krasnov, D.; Boeck, T. and Bühler, L.; "Turbulent and transitional sidewall jets in magnetohydrodynamic channels with a homogeneous magnetic field," Proceedings in Applied Mathematics and Mechanics, vol. 17, pp. 111-114, 2017.

[30] Mistrangelo, C. and Bühler, L.; "Instabilities in electrically driven rotating MHD layers," IOP Conference Series: Materials Science and Engineering, vol. 228, p. 012004, 2017.